Current and Future Aspects of Cancer Diagnosis with Positron Emission Tomography: Biological and Clinical Aspect

IV. 1   Current and Future Aspects of Cancer Diagnosis with Positron
         Emission Tomography: Biological and Clinical Aspect

Matsuzawa T., Fukuda H., Abe Y., Fujiwara T., Yamaguchi K., Ito M., Kubota K.,
Hatazawa J., Ito K., Sato T., Fares Y., Watanuki S., Sugawara Y., Tada M.*,
Komatsu K.*, Ido T.**, Iwata R.**, Ishiwata K.**, Takahashi T.** and Monma M.**
Group of Medicine, Tohoku University
Group of Chemistry, Tohoku University*
Group of Pharmacology, Tohoku University**

§ Why PET Now for Cancer Diagnosis?

At present, final cancer diagnosis is carried out morphologically under
the microscope.   Since this method is based on the examiner's subjectivity,
mistakes are unavoidable. In addition, information on the spreading of cancer
cannot be obtained at all by this method.   The development of an objective
method for cancer diagnosis that provides information on its spreading extent
is eagerly expected.

Using PET, we can obtain quantitative images of the metabolism of viable
cells.   What is better, the spreading extent of cancer can be detected easily
with PET, because cancer cells can be labelled with positron emitters which
irradiate two γ-rays in opposite directions following the extinction of the
positron.   In addition, if we can distinguish metabolic and histological
differences of cancer cell with PET, PET is to be the best method for cancer
diagnosis.   Schematic representation of the reason why PET now for cancer
diagnosis is illustrated in Fig. 1.

§ The Directions to Develop Cancer Diagnostic Positron Emitters[1-5]

In general, cancer cells have two characteristic natures.   One is an
intensive proliferating capacity, and the other is undifferentiation with
non-selective capacity for metabolic materials. In other words, it is thought
that cancer cells are hungry for metabolic materials such as sugars, amino
acids, and nucleic acids, because of their intensive proliferating capacity.
On the other hand, cancer cells are considered blind towards metabolic
materials because of their non-selective capacity for them.

We can catch starved and blind fish with baits ! Fishing cancer with
baits, such as false sugars, false amino acids, and false nucleic acids
labelled with positron, is our basic idea in developing cancer diagnostic
emitters as shown Fig. 2.

Using these positron emitters, in combinations of two or more, we could
detect quantitatively cancer metabolic type, and furthermore we can identify
its histology.   We found large cell carcinoma to have the highest ^{11}C-amino

acids uptake, followed by squamous cell carcinoma, while adenocarcinoma has the least uptake. Thyroid carcinoma has the highest uptake of ^{18}FDG followed by squamous cell carcinoma, and small cell carcinoma, in that order.

These findings will enable us in the future to make clear characteristic of cancer cells by studying their metabolism, and to draw up treatment protocols. Positron emitters permit us to make quantitative, and objective diagnosis of cancer, not only of its spreading extent, but also of its metabolic type, and malignancy. With the advent of multi-slice tomographic devices, with high resolution, this goal of cancer diagnosis coupled with appropriate treatment will be possible.

§ Biological and Clinical Studies with Positron Labelled False Sugars

As mentioned above, positron labelled false sugars are thought to be good tracers for cancer detection.

Radiopharmaceuticals

In this study, we used 5 hexose analogs, 2-deoxy-2-[F-18]fluoro-D-glucose (^{18}FDG), 2-deoxy-2-[F-18]fluoro-D-mannose (^{18}FDM)[6], 2-deoxy-2-[F-18]fluoro-D-galactose (^{18}FDGal), 2-deoxy-2-[F-18]fluoro-D-altrose (^{18}FDA) and 2-deoxy-2-[F-18]fluoro-L-glucose (L-^{18}FDG). Chemical structures of these compounds are shown in Fig. 3. Details of synthetic method, radiochemical yields and specific activities were described in another paper.[7,8]

Biological Study

Male Donryu rats (weighing 140-160 g) were used for tissue distribution studies. Transplantable hepatoma cells (AH109A) were subcutaneously inoculated into the back of the rats and were grown. When tumor size reached 1 cm in diameter, the experiments were done. Ten µCi of each compound was injected through lateral tail vein. The rats were killed by neck dislocation at 10, 30, 60 and 120 min after injection. The organs and tumor were removed, blotted, weighed and the radioactivities were counted by NaI well counter. Tissue uptake was expressed as percentage injected dose per gram of tissue (% dose/g).

An autoradiogram of tumor bearing rat was made after 2 mCi injection of ^{18}FDG or ^{18}FDGal. The rat was killed at 30 min after injection and freezed in dry-ice acetone. Thin sections (40 µm in thickness) were made with an autocryotome and contacted to the film for ^{3}H which was pre-cooled at -20°C. The films were exposed for 6-12 hours in a dark room at -20°C and then developed.

Positron emission tomogram of the tumor (VX7) bearing rabbit was taken using ECAT-II with medium resolution data aquisition mode and medium resolution filter function.

Fig. 4 shows tissue distribution of the compounds. Tumor uptake of [18]FDG was increased gradually and reached a plateau and remained constant during the study period. Liver uptake was initially high, however, decreased with time. Blood clearance was also very rapid. Tumor uptake of [18]FDM was almost the same as that of [18]FDG with more rapid blood clearance. Liver uptake of [18]FDM was also as low as that of [18]FDG. [18]FDGal accumulated much and trapped in the liver with less tumor uptake than that of [18]FDG and [18]FDM. On the other hand, [18]FDA and L-[18]FDG did not accumulate in and were washed out from any tissues including tumor.

Table 1 shows tumor uptake at 60 min, tumor-to-tissue ratios and tumor-to-blood ratios of these compounds. Tumor uptake of [18]FDG and [18]FDM were very high (2.65 % dose/g) and tumor-to-liver, pancreas and blood ratios of [18]FDG and [18]FDM were 18.9, 12.0, 22.1 and 9.2, 12.6, 29.4, respectively. Tumor uptake of [18]FDGal was not so high (1.37 % dose/g) as those of [18]FDG and [18]FDM, however, tumor-to-muscle ratio were highest (13.7) among these compounds.

Fig. 5 shows an autoradiogram with [18]FDG of a rat in which hepatoma cells were directly inoculated into the liver. Extremely high radioactivities were observed in the tumor which was clearly separated from the normal liver.[9]

Fig. 6 shows an autoradiogram of a rat with [18]FDGal.[10-12] High activity was seen in the liver and kidney which was consistent with biodistribution data. Subcutaneous tumor in the back of the rat was clearly separated from surrounding soft tissues.

Fig. 7 shows a positron tomogram with [18]FDM of a tumor bearing rabbit. Large tumor with central necrosis could be seen and metastatic lymphnodes were also cearly delineated.

From our experimental studies, [18]FDG was found to be a good radiopharmaceutical for abdominal and chest cancer detection. Advantages of [18]FDG for the use of cancer detection are as follows: (1) High tumor uptake and tumor-to-blood ratio can be obtained within a short time after injection. (2) Intrahepatic tumor can be positively delineated. These advantages were confirmed in clinical cases.[13,14] Tissue distribution of [18]FDM was almost the same as that of [18]FDG. Consequently, [18]FDM may have the same advantages as those of [18]FDG. Efficacy of the use of [18]FDG and [18]FDM cancer detection should be tested in clinical cases.

Clinical Study

Experimental studies of ours[11,12,14] shows [18]FDG is a good tracer for cancer detection. We examined the feasibility of this technique in patients with hepatoma, metastatic liver cancer and pancreatic cancer which have been difficult to be positively delineated by routinely used tumor scan.

Three cases of hepatocellular carcinoma (hepatoma) and 2 cases of pancreatic cancer with or without liver metastasis were examined with [18]FDG by PET. After 4-10 mCi of [18]FDG injection, sequential scan for every 5 min was

performed for 40 to 60 min by ECAT-II(Ortec). ^{18}F radioactivity in the tissue and tumor was expressed by differential absorption ratio (DAR). The DAR[15,16] is defined as follows:

$$DAR = \frac{\text{tissue activity}(\mu Ci/g)}{\text{injected dose}(\mu Ci) \ / \ \text{body weight}(g)}$$

$$= \frac{\text{tissue activity (count/pixel)}}{\text{injected dose}(mCi) \ / \ \text{body weight}(kg)} \times \text{calibration factor}$$

* Count/pixel (ECAT) was converted to µCi/g by a cross calibration factor between ECAT, curimeter and well counter by an assumption that the density of the tissue was 1.0 g/ml.

Fig. 8(a) shows X-CT of a hepatoma case. Large low density area was seen in the right lobe. Fig. 8(b) shows a sequential tomographic image of this case. In the first image, ^{18}F radioactivity distributed in most of the liver with a slightly cold area in the frontal part of the right lobe. There was an increase of radioactivity in this part with time. On the other hand, the activity rapidly decreased from the normal part of the liver. Consequently, we could obtain a clear image of the tumor after 30-50 min after injection. There were less accumulation of the activity in the central part of the liver which was thought to be a necrotic area by X-CT. These data shows ^{18}FDG tumor scan will provide an information about the distribution of viability of the tumor.

Fig. 9(a) shows an X-CT of pancreatic cancer. An abnormal mass was seen in the head of the pancreas. Fig. 9(b) shows a positron tomogram of this case 50 min after ^{18}FDG injection. There was an accumulation of the activity in the pancreas head tumor. This is the first report which described about positive imaging of pancreatic cancer with ^{18}FDG. ^{11}C-methionine can be used for the diagnosis of pancreatic cancer, however, the tumor was shown as a decrease or loss of activity.[17,18] Fig. 10(a) shows an X-CT of pancreatic cancer with liver metastasis. Very high activity was seen in the metastatic tumor with less activity in the primary pancreatic tumor. This data suggest that metastatic tumor was more active than primary tumor in this case.

Fig. 11 shows time activity pattern of the tumor in the examined cases. Tumor uptake was expressed by DAR. The uptake of normal liver was initially high but decreased with time. On the other hand, there were increasing of radioactivity in most of cases. Consequently, we could obtain high ratio of tumor-to-liver and then clear images of the tumor after 40-60 min. However, tumor activity of a hepatoma case was nearly the same as that of normal liver. One of the possible explanation of this low uptake is that the hepatoma might be well differentiated and has less hexokinase activity as that of normal liver.

Therefore, it is considered that degree of the uptake of ^{18}FDG is reflecting the malignancy of the tumor. The uptake of the metastatic carcinoma is very high. Contrary, some of the primary hepatoma shows very low uptake of ^{18}FDG. It is very close to the uptake of normal liver.

In conclusion, we showed that intrahepatic tumors and pancreatic cancers could be positively delineated with ^{18}FDG by PET. This diagnostic technique will be useful for the localization of the tumor, evaluation of viability and biochemical activity of the tumor and evaluation of therapeutic effectiveness.

§ Biological and Clinical Studies with False and Physiological Positron-Labelled Amino Acids

Radiopharmaceuticals

^{11}C-methionine was synthesized by the modified method of Comer et al.[19] Other ^{11}C-labelled amino acids were synthesized following the method of R. Iwata et al.[20] The enzymatic synthesis of ^{13}N-labelled amino acids were developed by K. Ishiwata, R. Iwata, M. Monma and T. Ido.[21]

Biological Study

For purpose of finding out the most appropriate amino acid for positron diagnosis of cancer, we compared 11 types of ^{11}C-labelled amino acids and 2 types of ^{13}N-labelled amino acids by examining their uptake into rat tumor in vivo, as shown Table 2. It was ^{11}C-ACPC, synthesized firstly by Washburn[22], which showed the highest accumulation in the tumor, with 3.46 % dose/g 20 min after the administration. The second was ^{11}C-L-Methionine, with 2.74 % and the third was Leucine, with 2.20 %. ACPC also has the merit of not entering into the liver. We reached the conclusion that ^{11}C-ACPC is the first amino acid for positron cancer diagnosis, and ^{11}C-L-Methionine is second.

We also carried out positron tomography using rabbit tumor and succeeded in visualizing the tumor clearly with both ^{11}C-ACPC and ^{11}C-Methionine, as shown Fig. 12.

Clinical Study

Fig. 13 shows PET images of human lung cancer with lymph node metastasis after injection of ^{11}C-L-Methionine. We can see many lymph nodes in lung cancer metastasis and its invasion into the thorax.

Fig. 14 also shows the image of human lung cancer after administration of ^{11}C-Methionine. The tumor is clearly visualized, however, unfortunately normal bone narrow is also visualized, because L-Methionine is a physiological metabolic agent. We are now planning to use the non-physiological amino acid, ^{11}C-ACPC for clinical study in the very near future.

§ Biological and Clinical Studies with Positron Labeled False Nucleic Acid-Fluorinated Pyrimidine[23-25]

Radiopharmaceuticals

The synthesis of ^{18}F-Labelled fluorinated pyrimidines was described elsewhere.[26] Chemical purity was more than 99 % and specific activity was 2.8-3.3 mCi/mg at the time of injection. Quality assurance tests of ^{18}FdUR for clinical use were performed according to the safety guidelines of the clinical research committee of our university.

Biological and Clinical Studies

A normal volunteer and four lung cancer patients, two with squamous cell carcinoma and two with small cell carcinoma. The study was approved by the clinical research committee of our institute and informed consent was obtained from all subjects. PET used was ECAT II. After transmission scans were performed using a ^{68}Ge ring source ^{18}FdUR (5-7 mCi) was injected IV as a bolus. Immediately after injection, continuous sequential scans were made at the fixed level. Each scan lasted 5 min. In a normal volunteer, rectilinear scan was done 90 min after injection.

Tumor uptake of ^{18}FUR was consistently less than that of either ^{18}FdUR or ^{18}F-5FU. The tumor uptake of ^{18}FdUR and ^{18}F-5FU were identical except for the period just after inoculation when ^{18}FdUR uptake surpasses ^{18}F-5FU uptake. Regarding tumor-to-organ ratios, the ratios obtained with ^{18}FdUR were always 1.3-4 times as large as those obtained with ^{18}FUR or ^{18}F-5FU. The rapid clearance in normal organs and slow clearance in the tumor resulted in the increased tumor-to-organ ratio with time. Our results proved that ^{18}FdUR is a suitable radiopharmaceutical for tumor imaging due to its sufficient uptake and the tumor-to-organ ratio obtained when using it. In the case of clinical application, while it is difficult to image the tumor localized on the chest, neck, and head.

Table 3(a)-(c) shows tissue distribution of three fluorinated pyrimidine in AH109A-bearing rat. Tumor uptake of ^{18}FdUR and ^{18}F-5FU were similar. Tumor uptake of ^{18}FUR was the lowest. Tumor-to-organ ratio of ^{18}FdUR was higher than that of ^{18}F-5FU and ^{18}FUR, because of rapid clearance of ^{18}FdUR in normal organs expect spleen. (By permission of Ref. 23.)

Autoradiographic study of ^{18}FdUR in rat is illustrated in Fig. 15. Tumor localization on the back was clearly seen. Radioactivity in the liver, kidney, and small intestine was high. On the other hand, radioactivity in the lung, brain, and muscle was very low.

Fig. 16 shows the rate of ^{18}FdUR and ^{3}H-thymidine incorporation of the acid-insoluble fraction in tumor and organs. The acid-insoluble fraction increased up to 34 % two hours after administration of ^{18}FdUR.

Fig. 17 shows the tissue distribution of ^{18}FdUR in a normal volunteer. Most of radioactivity was seen in the liver and kidnies, and was excreted to the urine.

Fig. 18 shows the image of ^{18}FdUR in a lung cancer patient. In the first image, high radioactivity was seen in the tumor and great vessels en bloc, then, in the second image, the tumor was visible. Radioactivity of the tumor, however, was declining with time.

Table 4 is the tumor-to-lung and-soft tissue ratio of ^{18}FdUR at 30 min after injection in four cases. First three tumors were clearly visible and easily distinguished from the surrounding tissues. But the last tumor was not clearly visible and its uptake was almost equivalent that of the soft tissues.

Clinical study with normal volunteer also reveal high radioactivity in the liver and kidney. Since it is difficult to detect the cancer located on the abdomen with PET like animal study, we began to examine the lung cancer. We studied four lung cancer patients, three of four cancers were positively imaged and one of four was scarcely imaged. Tumor uptake varies from patient to the other. ^{18}F-2-fluoro-2-deoxy-D-glucose(^{18}FDG) and ^{11}C-methionine which are other positron labelled tumor tracing agents indicate the glucose and amino acid metabolism of the tumor, respectively. Since ^{18}FdUR was incorporated into nucleic acid metabolism of the tumor, the tumor uptake of this radiopharmaceutical is different from that of ^{18}FDG and ^{11}C-methionine.

^{18}FdUR may indicate the nucleic acid metabolism of the tumor. But the quantitative analysis relating the rates of incorporation to the nucleic acids is not yet done. We are considering what types of tumor take ^{18}FdUR much or less and are studying the relationship between the tumor uptake of ^{18}FdUR and the proliferation.

§ Metabolic and Histological Diagnosis Using Combinations of Positron Emitters

Using these positron emitters in combinations of two or more we succeeded in developing the best cancer diagnostic method at present which enables us, not only to find its spreading, but also to detect quantitatively, its type, and degree of metabolism and furthermore its histology.

Fig. 19 shows the degree of uptake of ^{11}C-MET into human lung cancer as a function of time.

       1-5 squamous cell carcinoma   6-8 large cell carcinoma

       9   adenocarcinoma

The highest uptake was by large cell carcinoma, following by squamous cell carcinoma and adenocarcinoma had the least uptake.

Fig. 20 shows the uptake of ^{18}F-FDG into lung cancer. The ordinate shows the relative uptake into DAR and the abscissa shows the time after the administration of ^{18}F-FDG.

1-3 squamous cell carcinoma   4-5 adenocarcinoma
              6   small cell carcinoma   7   thyroid cancer
The highest uptake was by the thyroid cancer, the next was by squamous cell
carcinoma, followed by adenocarcinoma, and the least was by small cell
carcinoma. Using these two materials in combination, it is possible to
classify various histological types of cancer according to their metabolism.
Moreover, if ^{18}F-FdUR is used in addition to ^{11}C-Amino Acids and ^{18}F-FDG,
confidence in the diagnosis of histology will become even higher with the rare
exception of brain uptake of ^{18}F-FDG and pancreas uptake of ^{11}C-ACPC.
However, the problem is resolved by the use of combination of positron
emitters as explained above.

Rational Treatment Protocol and Future Prospects

        Using positron emitters in combinations of two or more, we are able to
make clear characteristics of cancer cells by their metabolism and to draw up
a protocol for rational treatment. Inhibiting, or even depriving the
neoplastic cells from their metabolic needs, based on the above diagnosis with
positron emitters, may be the key for rational treatment protocols in the
future, the advent of multi-slice tomographic devices of high resolution will
make the diagnosis with PET useful for clinical practice.
        In conclusion, our basic idea: "Fishing cancer with baits" is very
simple, but we believe it is fruitful.

§ Estimation for Undifferentiation of Cancer Cell and Detection of
    Primary Site of Cancer

        "Fishing cancer with baits" is our basic idea in developing cancer
diagnostic positron emitters.
        Our idea could be extended on both to estimate undifferentiation of
cancer cell as mentioned above and to detect primary site of cancer.
        Fig. 21 illustrates a schematic representation of various enzymatic
activities against undifferentiation in hepatocellular cancer.
        With increasing undifferentiation of cancer cell, hexokinase activity
decrease and phosphatase activity increase. Based on our basic studies, it is
thought that hexokinase activity is reversely proportional to phosphatase
activity. However galactokinase activity maintains pretty high value even
with increasing undifferentiation hepatocellular cancer. The highest
galactokinase activity is found in parenchymal cell of normal liver in our
studies.
        It is logical to believe that galactokinase is a characteristic enzyme in
liver cell. Therefore we are able to detect the primary site of
hepatocellular cancer with ^{18}FDGal.
        The detail of the detection of primary site of hepatocellular cancer will
be described of this proceeding in the next paper.

§ Can We Use Sokoloff's Model[27] in Cancer Study?

The correlation between [18]FDG uptake and blood glucose concentration in rats was investigated as described in the separate paper[28] of this proceeding.

Strong metabolic demand for glucose is apparently one of the common characteristics of the brain and tumor. However uptake of glucose for each is clearly distinct. The uptake of the brain decreased linearly with increasing blood glucose, revealing a strong negative correlation between brain uptake and blood glucose. The correlation coefficient was -0.86 and equation for the regression line was $y = -0.018x+4.8$.

Contrary, the tumor uptake pattern remained unchanged, irrespective of blood glucose level as shown Fig. 22.

We have faced the difficulty to use Sokoloff's model for obtaining absolute value quantitatively in cancer diagnosis with PET. Based on our observations, relative value as DAR (differential absorption ratio) or dose 1 g are sufficient for cancer diagnostic PET studies.

To obtain absolute value, we have to take blood sample from the artery of the patients frequently. The technique is bloody and the patients have to endure the pain stoically during examination.

It is thought that cancer diagnosis with PET should become to clinical examination in the near future. We have to choose useful value which minimizes patient's pain for clinical practice.

References

1) Matsuzawa T., Ido T., Hoshino F. et al, Abstract of Research Project, Grant-in-Aid for Scientific Research (A) from the Ministry of Education, Science and Culture, Japan (1979-1981) (in Japanese).

2) Matsuzawa T., Fukuda H., Ito M. et al., Japanese Journal of Clinical Medicine 42, 7 (1984) 207 (in Japanese).

3) Matsuzawa T., Fukuda H., Yamada K. et al., Oncologia 8 (1984) 29 (in Japanese).

4) Matsuzawa T., Ito M., Fukuda H. et al., The Journal of Accelerator Science and Technology 1, 1 (1984) 43.

5) Matsuzawa T., Fukuda H., Abe Y. et al., Clinic All-Round 34 (1985) 2734 (in Japanese).

6) Ido T., Wan C. N., Casella V. et al., Journal of Labelled Compounds and Radiopharmaceuticals 14 (1978) 175.

7) Takahashi T., Ido T., Iwata R. et al., CYRIC Annual Report (1981) 150.

8) Tada M., Matsuzawa T., Ohrui H. et al., Heterocycles 22 (1984) 565.

9) Fukuda H., Matsuzawa T., Abe Y. et al., European Journal of Nuclear Medicine 7, (1982) 294.

10) Fukuda H., Matsuzawa T., Tada M. et al., European Journal of Nuclear Medicine 11 (1986) 444.

11) Ishiwata K., Imabori Y., Ido T. et al., Japanese Journal of Nuclear Medicine 22 (1985) 1142.

12) Bauer C. H. et al., Cancer Research 40 (1980) 2026.

13) Yonokura Y., Benua R. S., Bill A. B. et al., Journal of Nuclear Medicine 23 (1982) 1133.

14) Fukuda H., Ito M., Matsuzawa T. et al., CYRIC Annual Report (1983) 244.

15) Moore F. D. et al., Journal of Clinical Investigation 22 (1943) 161.

16) Marrian D. H. et al., Br. Journal of Cancer 10 (1956) 575.

17) Fukuda H., Matsuzawa T., Ito M. et al., Experimental and Clinical Study of Cancer Diagnosis with ^{18}F-FDG Using Positron Emission Tomography, 31st Annual Meeting of the Society of Nuclear Medicine, June 5-8, Los Angeles (1984) 50.

18) Syrota A. et al., Radiology 143 (1982) 249.

19) Comer D. et al., European Journal of Nuclear Medicine 1 (1976) 11.

20) Iwata R., Takahashi T., Ido T. et al., CYRIC Annual Report (1982) 111.

21) Ishiwata K., Iwata R., Monma M. et al., CYRIC Annual Report (1981) 146.

22) Washburn L. C. et al., Journal of Nuclear Medicine 17 (1976) 748.

23) Abe Y., Fukuda H., Ishiwata K. et al., European Journal of Nuclear Medicine 8 (1983) 258.

24) Ishiwata K., Ido T., Abe Y. et al., European Journal of Nuclear Medicine 10 (1985) 38.

25) Abe Y., Matsuzawa T., Ito M. et al., Japanese Journal of Nuclear Medicine 22 (1985) 583.

26) Ishiwata K., Monma M., Iwata R. et al., Journal of Labelled Compd. Radiopharm. 21 (1984) 1231.

27) Sokoloff L., Reivich M., Kennedy C., et al., Journal of Neuro chemistry 28 (1977) 897.

28) Yamada K., Endo S., Fukuda H. et al., European Journal of Nuclear Medicine 10 (1985) 341.

Table 1. Tumor uptake and tumor-to-tissue ratios in F-18 deoxyfluoro
          hexoses in hepatoma (AH109A) bearing rats.

Compound	Tumor uptake	Tumor-to-tissue ratio			
		blood	muscle	liver	pancreas
^{18}FDG	2.65+0.61	22.1	6.5	18.9	12.6
^{18}FDM	1.65+0.81	29.4	5.4	9.1	12.6
^{18}FDGal	1.37+0.17	5.3	13.7	0.2	—
^{18}FDA	0.50+0.08	1.4	1.6	0.9	1.4
^{18}L-FDG	0.30+0.03	1.1	3.3	1.3	1.7

Table 2. Comparative study of cancer diagnosis using positron
          labelled amino acids.
          Tumor uptake of various radiolabeled amino acids in
          male Donryu rats, bearing hepatoma AH109A.

Compounds	Rat numbesr	Tumor uptake at 20 min. (% Dose/g)	Tumor-to-organ ratio					
			Blood	Liver	Brain	Lung	Myo-cardium	Skeletal Muscle
^{11}N–L–glutamic acid	(5)	1.34±0.47	4.50	0.80	5.60*	1.38*	1.24	1.23*
^{11}N–L–alanie	(2)	1.02±0.08	2.76	0.48	3.92	0.83	0.82	—
→^{11}C–L–methionine	(5)	2.74±0.36	11.40	0.60	6.33*	1.93*	4.70	5.38
—^{11}C–D.L-leucine	(5)	2.20±0.21	2.85	0.89	4.00	1.94	2.39	—
^{11}C–D.L–valine	(5)	2.02±0.18	1.15	0.70	2.50	—	1.43	—
^{11}C–D.L-phenylalanine	(5)	1.42±0.25	3.32	0.77	4.43	2.03	2.67	—
^{11}C–D.L-phenylglycine	(5)	1.40±0.31	2.08	1.82	5.28	1.92	2.36	—
^{11}C–D.L–norleucine	(5)	1.56±0.13	2.01	1.55	3.72	1.63	1.88	—
^{11}C–D.L-clclohexylglycine	(5)	1.24±0.09	1.77	1.61	2.55	1.63	1.70	1.71
→^{11}C-ACPC	(7)	3.46±0.16	4.63	2.29	4.02*	3.20	3.43	3.92
^{11}C-methyl ACPC	(3)	1.79±0.12	2.67	2.52	3.52	2.58	2.22	2.02
^{11}C-ACHC	(6)	1.32±0.11	1.21	1.06	3.37	1.43	1.78	2.40
^{11}C-methyl ACHC	(5)	1.02±0.13	1.14	1.42	3.45	1.52	1.68	1.89

*Data from separate experimens.

Table 3(a). Tissue distribution of ^{18}F-FUR in tumor-bearing rats.

organ	10min.	30min.	60min.	120min.
Blood	0.60±0.07 (0.96)	0.39±0.09 (1.91)	0.19±0.06$^{@}$ (3.49)	0.06±0.03* (5.90)
Heart	0.51±0.08 (1.15)	0.38±0.07$^{@}$ (1.95)	0.23±0.06$^{@}$ (2.87)	0.09±0.03$^{@}$ (4.13)
Lung	0.59±0.08 (0.98)	0.52±0.07$^{@}$ (1.45)	0.34±0.10$^{@}$ (1.92)	0.21±0.09$^{@}$ (1.74)
Liver	7.47±0.83 (0.08)	4.57±1.30 (0.16)	1.96±0.80 (0.34)	0.77±0.18* (0.49)
Kidney	8.17±1.65$^{@}$ (0.07)	14.27±2.10$^{@}$ (0.05)	7.73±2.90* (0.09)	2.65±0.96$^{@*}$ (0.14)
Spleen	0.46±0.08$^{@}$ (1.26)	0.43±0.08 (1.73)	0.31±0.09 (2.15)	0.16±0.05$^{@*}$ (2.35)
Muscle	0.43±0.07 (1.34)	0.22±0.03 (3.36)	0.14±0.04$^{@}$ (4.83)	0.10±0.05$^{@}$ (3.61)
Brain	0.09±0.01$^{@*}$ (6.81)	0.08±0.01$^{@}$ (9.22)	0.06±0.01$^{@*}$ (10.27)	0.04±0.01$^{@}$ (10.63)
Tumor	0.58±0.20$^{@}$	0.75±0.21	0.66±0.19	0.37±0.09$^{@}$

Table 3(b). Tissue distribution of ^{18}F-5-FU in tumor-bearing rats.

organ	10min.	30min.	60min.	120min.
Blood	0.61±0.09 (1.22)	0.42±0.08 (2.20)	0.22±0.08$^{\#}$ (3.68)	0.10±0.02$^{*\#}$ (6.34)
Heart	0.51±0.09 (1.45)	0.38±0.08 (2.44)	0.22±0.08$^{\#}$ (3.68)	0.11±0.02$^{\#}$ (5.77)
Lung	0.60±0.09 (1.23)	0.49±0.10$^{\#}$ (1.88)	0.38±0.11$^{\#}$ (2.17)	0.30±0.07$^{\#}$ (2.15)
Liver	8.87±1.69$^{\#}$ (0.08)	5.80±1.36$^{\#}$ (0.16)	2.65±0.75$^{\#}$ (0.30)	1.21±0.19$^{*\#}$ (0.53)
Kidney	10.14±1.38$^{\#}$ (0.07)	15.55±5.18$^{\#}$ (0.06)	13.80±5.48$^{\#}$ (0.06)	5.81±1.37$^{*\#}$ 90.11)
Spleen	0.50±0.06$^{\#}$ (1.47)	0.52±0.11 (1.75)	0.37±0.10 (2.19)	0.24±0.03$^{*\#}$ (2.72)
Muscle	0.43±0.02 (1.67)	0.26±0.05 (3.57)	0.16±0.05$^{\#}$ (5.22)	0.12±0.01$^{\#}$ (5.16)
Brain	0.10±0.01$^{*\#}$ (7.17)	0.09±0.01$^{\#}$ (9.73)	0.08±0.02$^{*\#}$ (10.24)	0.06±0.04$^{\#}$ (10.85)
Tumor	0.74±0.19$^{\#}$	0.92±0.15	0.81±0.24	0.64±0.34

Table 3(c). Tissue distribution of ^{18}F-FdUR in tumor-bearing rats.

organ	10min.	30min.	60min.	120min.
Blood	0.56±0.07 (1.83)	0.33±0.06 (2.90)	0.12±0.06[@#] (6.12)	0.03±0.01[#] (18.27)
Heart	0.52±0.08 (1.94)	0.29±0.06[@] (3.32)	0.11±0.04[@#] (6.46)	0.05±0.01[@#] (11.38)
Lung	0.51±0.10 (2.00)	0.30±0.08[@#] (3.20)	0.16±0.03[@#] (4.46)	0.10±0.03[@#] (6.15)
Liver	6.92±0.66[#] (0.15)	3.67±1.19[#] (0.26)	1.43±0.31[#] (0.49)	0.60±0.08[#] (1.01)
Kidney	5.76±0.87 (0.17)	8.49±3.05[@#] (0.11)	4.31±1.96[#] (0.16)	0.94±0.20[@#] (0.64)
Spleen	0.72±0.11[@#] (1.40)	0.63±0.31 (1.52)	0.40±0.10 (1.78)	0.50±0.08[@#] (1.20)
Muscle	0.44±0.05 (2.33)	0.21±0.05 (4.59)	0.08±0.03[@#] (8.80)	0.03±0.01[@#] (17.13)
Brain	0.06±0.02[@#] (16.67)	0.05±0.01[@#] (19.28)	0.04±0.01[@#] (18.53)	0.02±0.00[@#] (33.50)
Tumor	1.02±0.19[@#]	0.96±0.24	0.70±0.06	0.60±0.17[@]

Table 4. Tumor-to-organ ratio of ^{18}FdUR at 30 min.

Case	Ratio	
Lung cancer	soft tissue	lung
small cell carcinoma	3.01	13.25
squamous cell carcinoma	2.14	8.71
small cell carcinoma	1.95	4.82
squamous cell carcinoma	1.15	4.94

Why PET now for cancer diagnosis ?
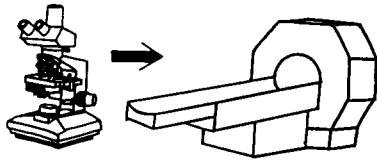
1. subjective ——→ objective

2.   image
   qualitative ——→ quantitative

3.   spreading
   no information ——→ information

4.   histological difference
   can be   to be
   ——→
   distinguished   distinguished

baits

false { sugars
       { amino acids
       { nucleic acids

almost blind

hungry

T.Matsuzawa

Fig. 1.   Fig. 2.

[^{18}F]-2-DEOXY-2-FLUOROHEXOPYRANOSES

D-Glucose der.   D-Galactose der.   D-Gulose der.   D-Allose der

D-Mannose der.   D-Talose der.   D-Idose der.   D-Altrose der.

L-Glucose der.
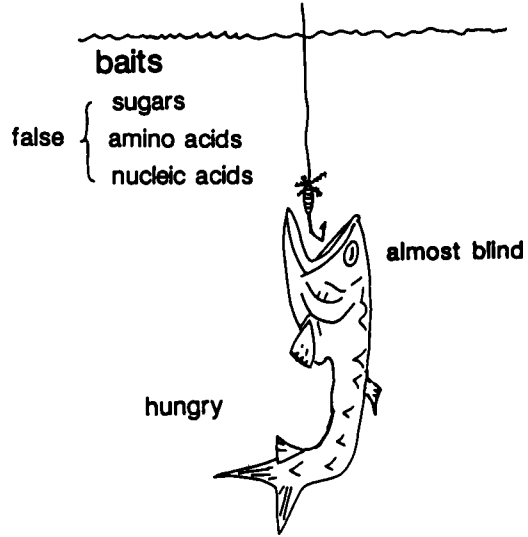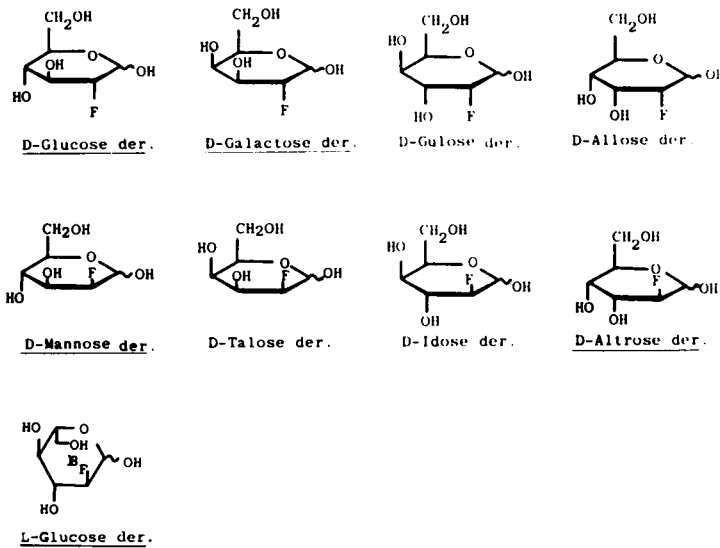
Fig. 3. Chemical structure of ^{18}F-2-deoxy-2-fluorohexoses. Underlined compounds were obtained and tested for tissue distribution studies.
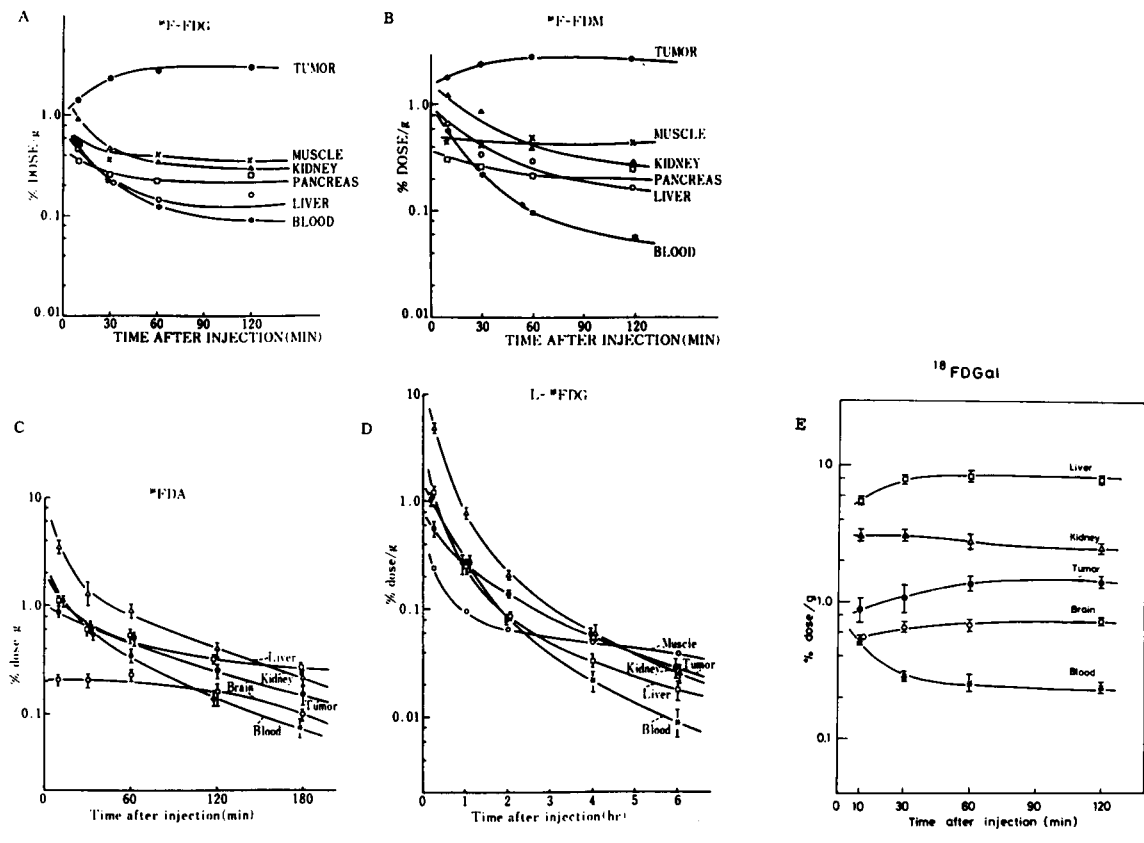
Fig. 4. Tissue distribution of ^{18}F-2-deoxy-2-fluorohexoses in hepatoma (AH109A) bearing rats.

Fig. 5. Autoradiogram with ^{18}FDG in tumor bearing rat.
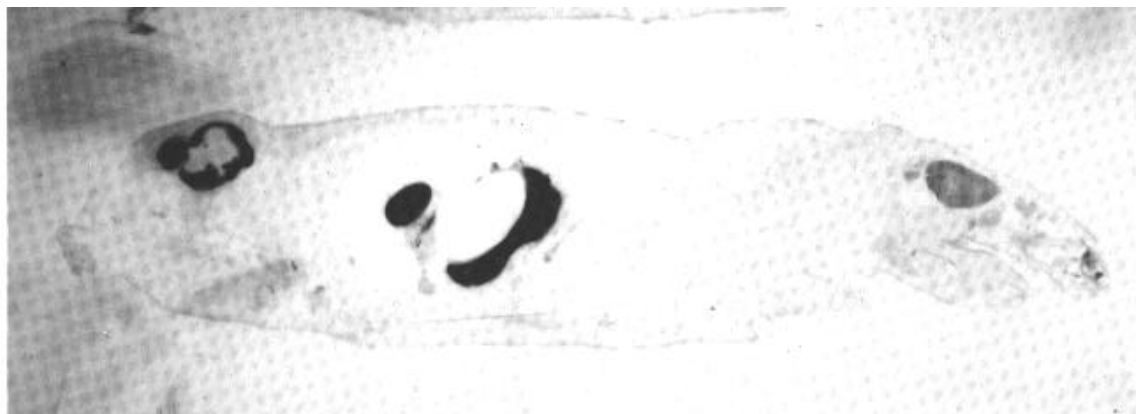
Fig. 6. Autoradiogram with ^{18}FDGal in tumor bearing rat.
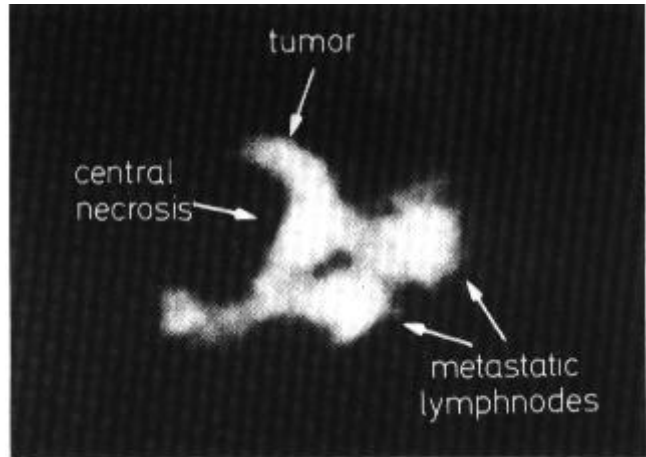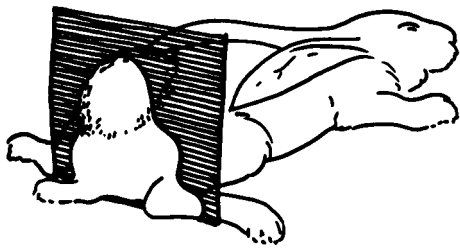
Fig. 7. Positron tomogram with ^{18}FDM in tumor bearing rabbit.
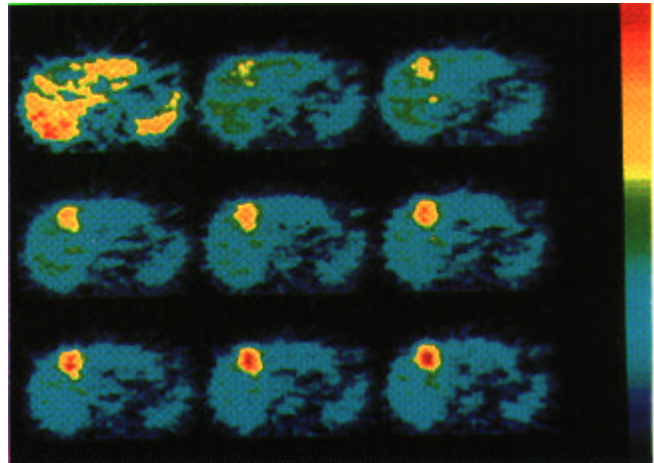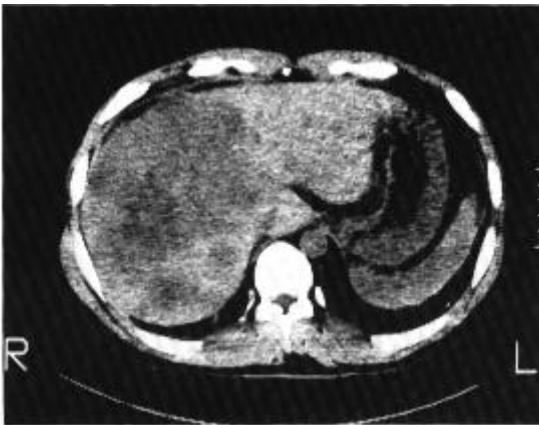
Fig. 8. (a) X-CT of a hepatoma case. Large low density area was seen in the right lobe. (b) Sequential tomogram of this case with ^{18}FDG. In the initial image, the activity distributed uniformly in the liver. There was an increase of activity in the frontal part of the liver.
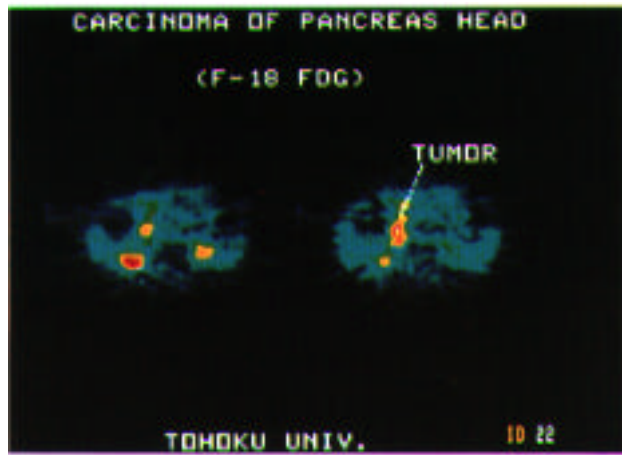
Fig. 9. (a) X-CT of a pancreatic cancer. An abnormal mass was observed in the head of pancreas. (b) Positron tomogram of this case 50 min after ^{18}FDG injection. High activity was seen in the head tumor. Bilateral kidney showed very high activity.
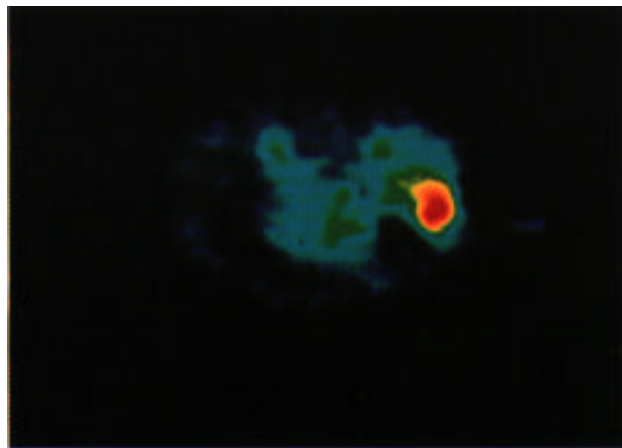
Fig. 10. (a) X-CT of a pancreatic cancer with liver metastasis. Low density area in the liver found to be a liver metastasis. (b) Positron tomogram of this case 50 min after ^{18}FDG injection. The activity of the metastatic liver tumor was much higher than that of primary pancreatic tumor.

Increased accumulation of ^{18}FDG in hepatoma
and pancreatic cancers as expressed by DAR
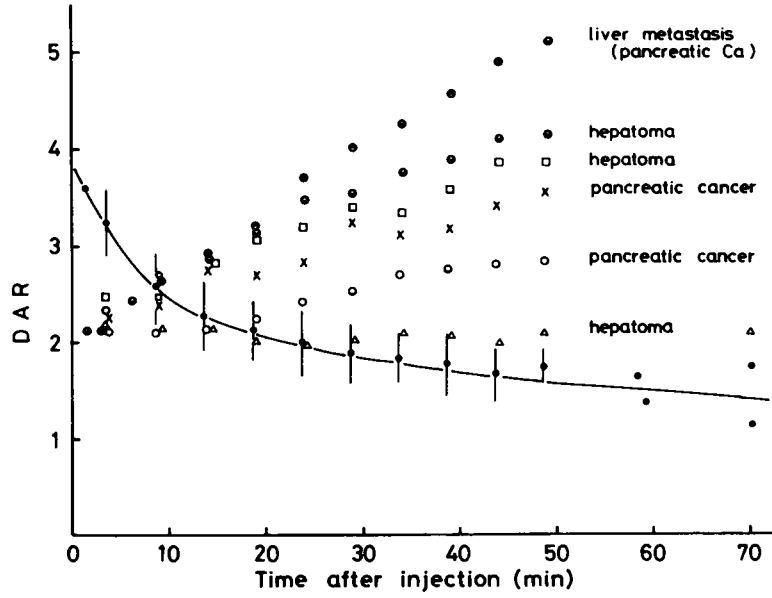
Fig. 11. Tumor uptake of examined cases. The uptake was expressed by
differential absorption ratio (DAR) as a function of time
after injection. Normal liver (●-●), case 1 (●), case 2 (x),
case 3 (o,⊖).

^{11}C-methionine

^{11}C-ACPC
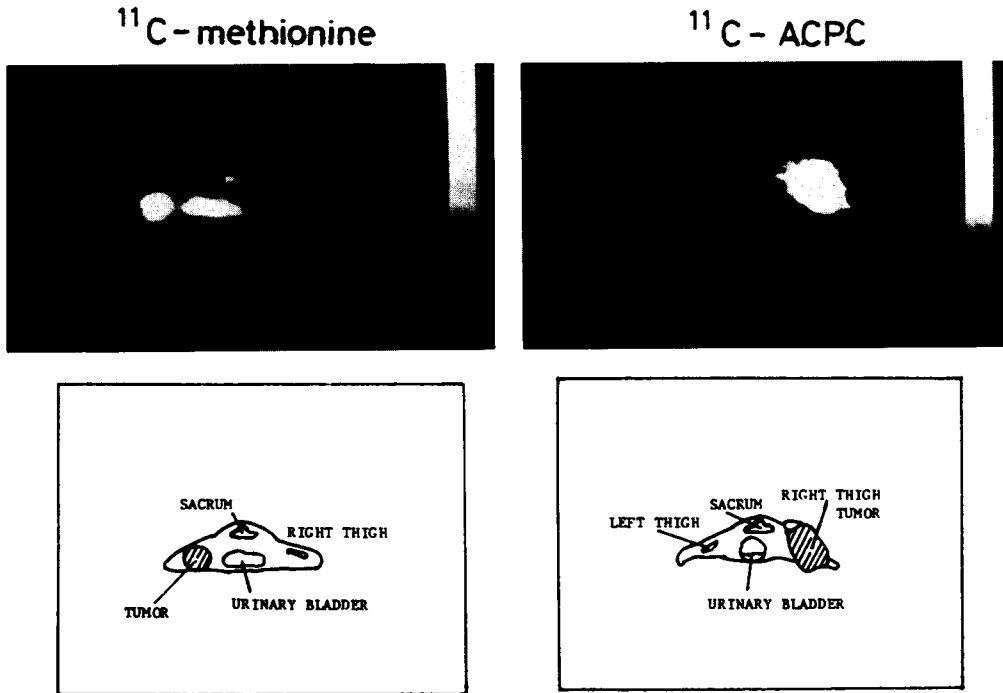
Fig. 12.
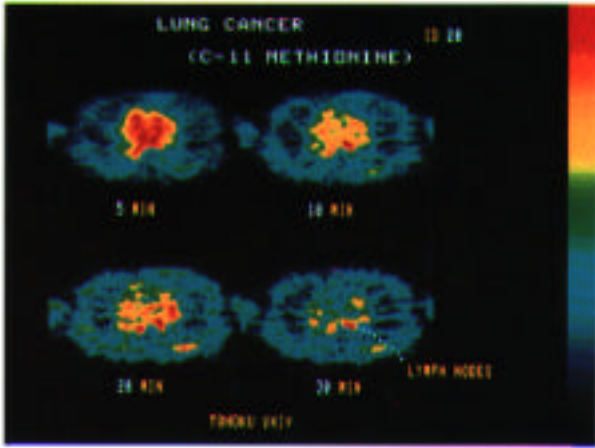
Fig. 13.
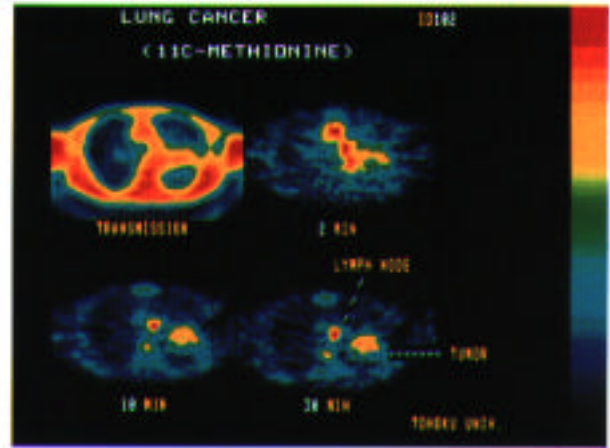
Fig. 14.

Fig. 15. Autoradiogram of a tumor bearing rat 60 min after injection of ^{18}FdUR. (By permission of Ref. 23.)
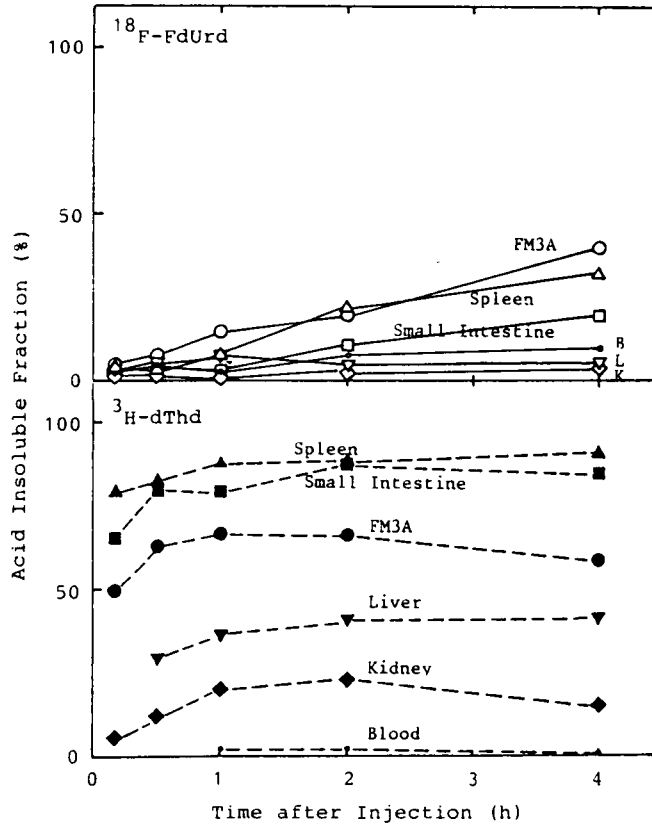
Fig. 16. [18]FdUR- and ^{3}H-TdR-incorporation into at acid insoluble
          fraction.
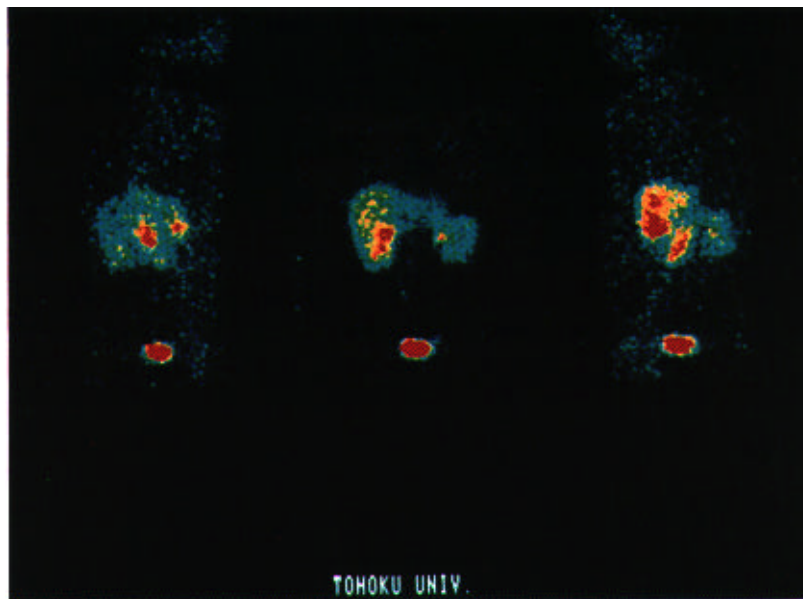
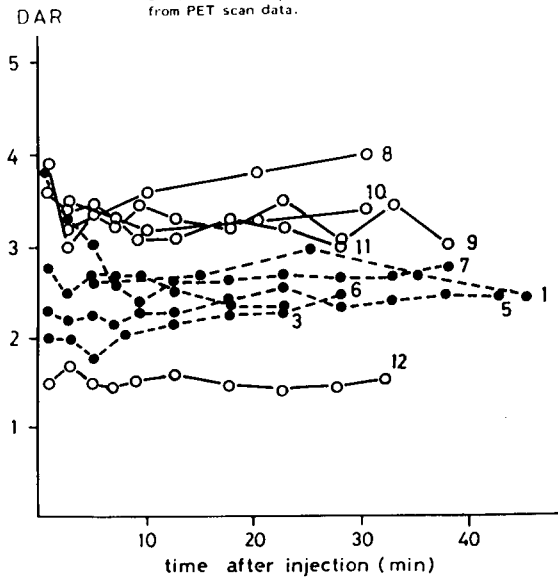Fig. 17. Rectilinear scan of normal volunteer 90 min after injection
of ^{18}FdUR.
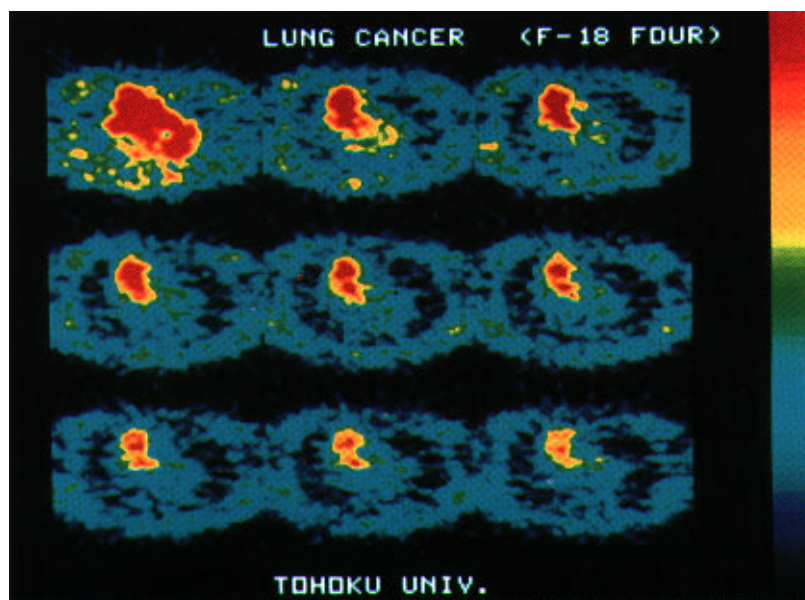
Fig. 18. Emission scan of lung cancer. Each scan lasted 5 min.

Time activity curves of lung tumor.
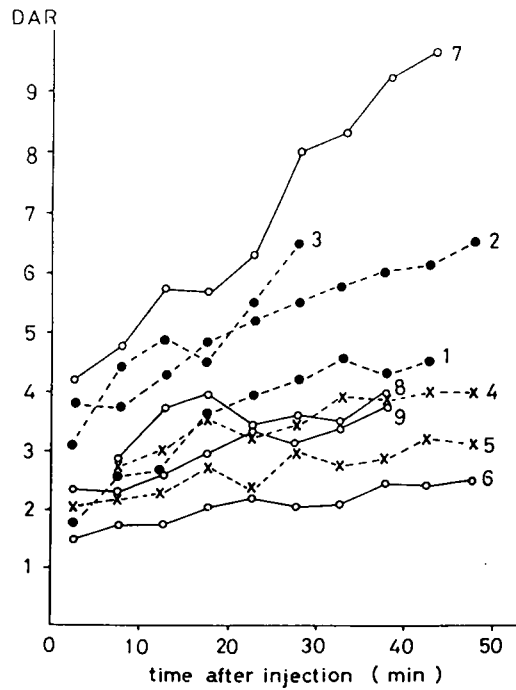Differential absorption ratios of the tumor were calculated
from PET scan data.

DAR (Differential Absorption Ratio)

$$= \frac{\text{ECAT Count}}{\text{Injected Dose} \times \text{Scan Time/Body Weight}} \times \text{Calibration factor}$$

Fig. 19. Uptake of ^{11}C-Methionine in lung cancer.

Time activity curves of lung cancers
Differential absorption ratios of the tumor were calculated
from PET scan data.

DAR (Differential Absorption Ratio)

$$= \frac{\text{ECAT Count}}{\text{Injected Dose} \times \text{Scan Time/Body Weight}} \times \text{Calibration factor}$$
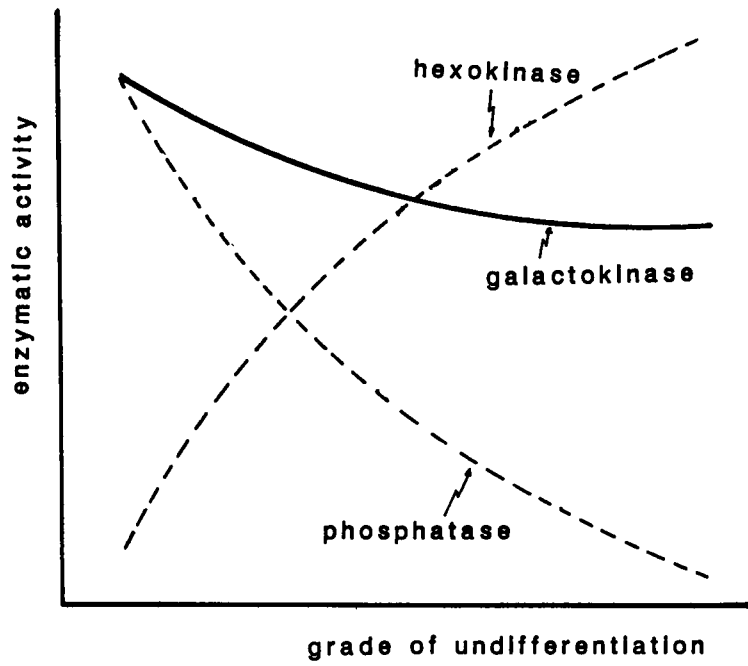
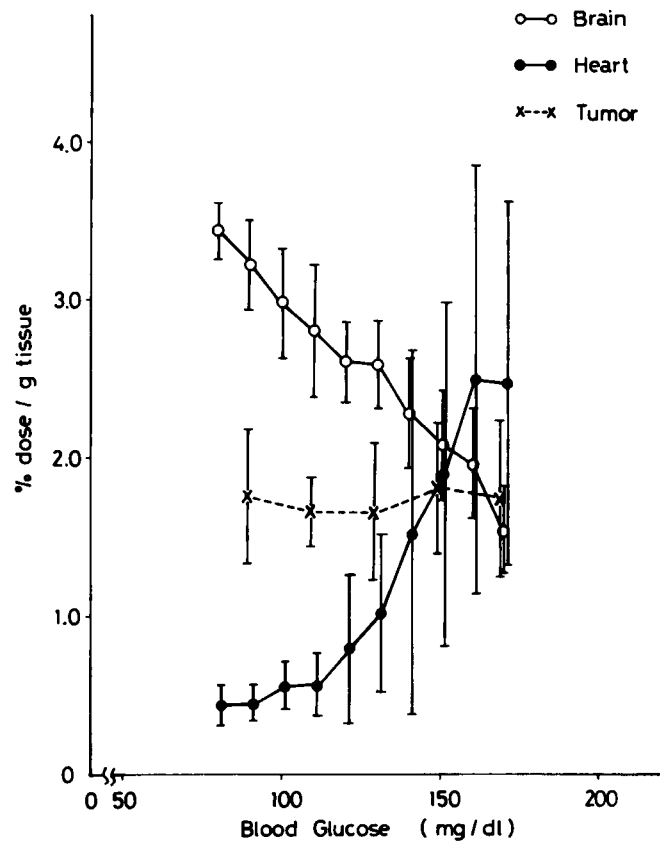Fig. 20. Uptake of ^{18}F-FDG.

Fig. 21.

Fig. 22. Correlation between ^{18}F-FDG uptake and blood glucose
level.   o—o brain;   •—• myocardium;   x--x tumor.
Eachpoint represents mean ± SD.